Published in final edited form as:

J Orthop Res. 2017 August ; 35(8): 1699–1706. doi:10.1002/jor.23440.

Osteoclast Depletion with Clodronate Liposomes Delays Fracture Healing in Mice

Hsuan-Ni Lin, M.S., **J. Patrick O'Connor, Ph.D.**

Department of Orthopaedics, Graduate School of Biomedical Sciences and New Jersey Medical School, Rutgers, the State University of New Jersey, Newark, NJ 07103

Abstract

Osteoclasts are abundant within the fracture callus and also localize at the chondro-osseous junction. However, osteoclast functions during fracture healing are not well defined. Inhibition of osteoclast formation or resorptive activity impairs callus remodeling but does not prevent callus formation. Interestingly though, anti-osteoclast therapies differentially affect resolution of callus cartilage into bone. Treatments that inhibit osteoclast formation or viability tend to impair callus cartilage resolution, while treatments that target inhibition of bone resorption generally do not affect callus cartilage resolution. Here we tested whether depletion of osteoclasts by systemic treatment with clodronate liposomes would similarly impair callus cartilage resolution. ICR mice were treated by intraperitoneal injections of clodronate-laden liposomes or control liposomes and subjected to closed femur fracture. Femurs were resected at multiple times after fracture and analyzed by radiography, histology, and mechanical testing to determine effects on healing. Clodronate liposome treatment did not prevent callus formation. However, radiographic scoring indicated that clodronate liposome treatment impaired healing. Clodronate liposome treatment significantly reduced callus osteoclast populations and delayed resolution of callus cartilage. Consistent with continued presence of callus cartilage, torsional mechanical testing found significant decreases in callus material properties after 28 days of healing. The results support a role for osteoclasts in the resolution of callus cartilage into bone. Whether the cartilage resolution role for osteoclasts is limited to simply resorbing cartilage at the chondro-osseous junction or in promoting bone formation at the chondro-osseous junction through another mechanism, perhaps similar to the reversal process in bone remodeling, will require further experimentation.

Keywords

Fracture Healing; Bone Regeneration; Osteogenesis; Osteoclasts; Macrophages; Clodronate Liposomes; Mouse Model

Address correspondence to: J. Patrick O'Connor, Ph.D., Medical Sciences Building, room E-659, Rutgers-New Jersey Medical School, 185 South Orange Ave., Newark, NJ 07103, Tel: 973-972-5011, oconnojp@njms.rutgers.edu.

AUTHOR CONTRIBUTIONS: HNL contributed to this manuscript by performing the experiments, collecting data, analyzing the data, and editing the manuscript. POC conceived and designed the study, analyzed the data, prepared the manuscript, and approved the final version of the manuscript.

INTRODUCTION

Osteoclasts are abundant in the fracture callus and localize at the callus chondro-osseous junction during endochondral ossification[1]. Differentiation of osteoclasts from monocytes by M-CSF and RANKL stimulation is well established. In addition, trans-differentiation of macrophages into osteoclasts has been described[2–4]. The role of osteoclasts in fracture healing is thought to be limited primarily to resorption of calcified cartilage during callus endochondral bone formation and to bone resorption during callus remodeling. In fracture models, treatments that impair osteoclast activity also inhibit callus remodeling. There are 3 main classes of osteoclast inhibitory drugs, bisphosphonates (e.g., alendronate and zoledronic acid), denosumab which binds RANKL to prevent osteoclastogenesis, and odanacatib that inhibits cathepsin K[5]. These drugs differentially affect resolution of callus cartilage. Alendronate treatment does not appear to reduce callus osteoclast populations, but does delay cartilage resolution and remodeling[6–8]. Zoledronic acid does not appear to affect callus osteoclast populations or callus cartilage resolution but does inhibit callus remodeling[9; 10]. Denosumab treatment does reduce callus osteoclast populations and delays cartilage resolution and remodeling[6]. Odanacatib treatment appears to increase callus osteoclast populations, does not appear to affect cartilage resolution, but does inhibit remodeling[7; 8]. Thus it is unclear whether the delay in callus cartilage resolution is caused by loss of callus osteoclasts or inhibition of callus osteoclast activity.

We hypothesize that efficient resolution of callus cartilage requires the presence of osteoclasts, even if the resorptive activity of those osteoclasts is impaired. We tested this hypothesis by measuring the effects of systemic clodronate liposome (CLD-lip) treatment on fracture healing in mice. CLD-lips have been used in many studies to deplete monocyte-derived cell populations[11–13]. Clodronate is a non-nitrogenous bisphosphonate. Liposome encapsulated clodronate induces apoptosis in cells that endocytose the liposomes. Thus, CLD-lip treatment preferentially targets monocytes and monocyte-derived cells such as macrophages and osteoclasts. Depletion of monocytes also reduces the number of cells available for osteoclastogenesis. We found that callus formation occurred in the reduced presence of osteoclasts. However, we also found that resolution of callus cartilage into bone appeared to be impaired in the osteoclast-depleted fractures leading to a delay in bony bridging of the fracture. The results suggest that an interaction between callus chondrocytes and osteoclasts is necessary for efficient endochondral ossification during fracture repair.

MATERIALS & METHODS

Animal Model

Female ICR mice that were 10–12 weeks old and weighed 29.5 ± 2.4 g (mean ± SEM) were used (Taconic Farms, Inc. Germantown, NY). All animal procedures were approved by the Rutgers-New Jersey Medical School Institutional Animal Care and Use Committee. CLD-lips containing 5 mg/ml disodium clodronate and control liposomes in phosphate buffered saline (PBS-lip) were obtained from ClodronateLiposome.com (Amsterdam). Liposomes were injected intraperitoneally at 4 day intervals from 6 days before fracture until the animal reached its experimental endpoint and at a dose of 0.3 mls of liposomes. A closed, diaphyseal fracture was created in the right femur using a custom-made, three-point bending

device (BBC Specialty Automotive Center, Linden, NJ) as described previously except the mice were allowed to recover for 7 days between insertion of the intramedullary pin and production of the fracture[14]. Mice were euthanized at 4, 10, 14, and 21 days after fracture for histology and at day 28 for torsional mechanical testing. Femurs collected at 14 and 21 days after fracture were analyzed by micro-computed tomography (μCT) before histological analysis. No animals died or were euthanized prior to an experimental endpoint. All animals appeared healthy at the time of euthanization but no final body weight or other measure of overall animal health was recorded at the time of euthanization.

Femurs were quickly resected from mice, fixed in Streck Tissue Fixative (STF, Streck, Inc., Omaha, NE) for one day, and then decalcified in 10% EDTA for a week. Tissues for μCT analysis were scanned before decalcification. After decalcification, tissues were embedded in paraffin. Five micrometer thick sections were cut parallel to the long axis of the femur and through the intramedullary canal. Sections were deparaffinized in three changes of xylene and rehydrated in a graded alcohol series. Osteoclasts were detected by tartrate-resistant acid phosphatase (TRAP) staining as described previously[1]. TRAP stained sections were counterstained with hematoxylin (Sigma-Aldrich, St. Louis, MO). Cartilage was identified by safranin-O (Sigma-Aldrich) staining, and then counterstained with fast green (Sigma-Aldrich) and hematoxylin. Bone was identified using aniline blue, and then counterstained with biebrich scarlet-acid fuchsin and haematoxylin (Masson's trichrome stain; Sigma-Aldrich). Sections were mounted using Permount mounting medium (Fisher Scientific, Waltham, MA).

Image Collection and Analysis

Cartilage area, bone area, and the size of callus area were measured from digital images of each callus captured using an Olympus SZ-40 microscope (Olympus Corporation of America, Center Valley, PA) and a SPOT Idea camera (Diagnostic Instruments, Inc., Sterling Heights, MI). Measurements were made using Image-Pro software (version 9, Media Cybernetics, Inc., Rockville, MD). To measure TRAP positive ($TRAP^+$) cells per mm^2, tiled images of each histological specimen were captured with a Nikon DS-Fi1 digital camera using a Nikon Eclipse E800 microscope (Nikon Instruments Inc., Melville, NY). The tiled images for each specimen were combined into one continuous image that covered the entire callus using Adobe Photoshop CS5.1 (Adobe Systems Incorporated, San Jose, CA). $TRAP^+$ cells in the entire callus were manually counted and divided by callus area to generate number of TRAP positive cells per mm^2.

Mechanical Testing

Mice were euthanized at 28 days after fracture and femurs were resected. Femurs with oblique, comminuted, or infected fractures were not used for mechanical testing. Soft tissue was removed from the femur while leaving the fracture callus undisturbed. The femurs were wrapped in saline-soaked gauze and stored in −80°C until mechanical testing[15]. Femoral length, maximum and minimum fracture callus diameters, and maximum and minimum mid-diaphyseal diameters of intact femur were measured. After thawing, the intramedullary pin was removed and the femoral ends were potted in 1 cm hexagonal nuts using polymethylmethacrylate cement. The gauge length of the sample was measured after

potting. Samples were wrapped in saline-soaked gauze to prevent dehydration between steps. Torsional testing was conducted using a servo-hydraulic testing machine (MTS, Eden Prairie, Minnesota) with a 20 Nm reaction torque cell (Interface, Scottsdale, Arizona). Testing was carried out to failure at an actuator head displacement rate of 2° per second and a data recording rate of 20 Hz. Femurs were tested by internal rotation in proper anatomic orientation until failure. Internal callus dimensions were measured after torsional testing. The peak torque and the angle at the time of failure were obtained from the load-deformation curves. The femoral dimensions were used to calculate shear stress, shear modulus, and torsional rigidity as described previously[14; 16; 17].

Radiographic Analyses

Radiographs were made after fracture using a Faxitron MX-20 (Faxitron Bioptics, LLC, Tucson, AZ) and Kodak MIN-R 2000 mammography film (Carestream Health, Rochester, NY) to confirm the position and quality of each fracture and to assess healing. Fracture healing was graded using radiographs blinded for treatment and a 4-point scoring system as described previously[18]. The grading scheme was based on the bridging of the fracture by callus and the cortical bone at the fracture site. One point was assigned to each aspect of the fracture (the right callus and cortex and the left callus and cortex) that appeared bridged. A score of 0 represented the absence of radiographic bridging among all four aspects of the fracture, indicating a fracture nonunion. A score of 4 represented a fully bridged fracture.

For μCT analysis, femurs were fixed in STF and stored in 70% ethanol until scanning. Samples were scanned using a Skyscan 1172 (Skyscan, Kontich, Belgium) in saline, at a voxel size of 5 μm, X-ray tube voltage of 60 kV, X-ray tube current of 167 μA, and exposure time of 590 ms. X-ray projections were collected at 0.6± intervals over a total angular rotation of 205.8± with 2 frames averaged for each rotation. A 0.5 mm aluminum filter was used to reduce beam-hardening. Sizes for the scanned and reconstructed regions varied for each specimen but included the entire callus for each femur. Images were reconstructed into three-dimensional volumes using NRecon software (Skyscan) without Hounsfield correction using the automated setting of the NRecon software which gave a dynamic range from 0 to 0.125. A sagittal view of each callus was created using the CTVol software (Skyscan).

Statistical Analyses

All statistical analyses were performed using Sigmaplot version 12.5 software (Systat Software, Inc., San Jose, CA). Callus $TRAP^+$ cells counts were analyzed between groups by ANOVA and post-hoc Student-Newman-Keuls tests. Radiograph scores between the PBS-lip and CLD-lip groups were compared using Mann-Whitney Rank Sum Tests for each time point. Callus area, percent cartilage and percent bone data were analyzed by ANOVA and post-hoc Holm-Sidak tests.

RESULTS

Clodronate Liposome Treatment Reduces the Fracture Callus Osteoclast Population

Histochemical staining of fracture callus sections was performed to confirm that CLD-lip treatment reduced callus osteoclast numbers. Sections were prepared from CLD-lip and

PBS-lip treated mice at 4, 10, 14, and 21 days after fracture and stained for TRAP activity. At day 4 after fracture, $TRAP^+$ cells within the intramedullary canal adjacent to the fracture site were abundant in control PBS-lip treated mice but were almost absent in the CLD-lip treated mice (Figure 1A and B, Supplemental Data Figure S-1). At 14 days after fracture, fewer TRAP+ cells were apparent in the external fracture callus of the CLD-lip treated mice as compared to the PBS-lip treated mice (Figure 1C and D, Supplemental Data Figure S-1). $TRAP^+$ cells in the external callus were counted at days 10, 14, and 21 after fracture (Figure 1E; ANOVA $P < 0.001$). In the PBS-lip group, external fracture callus $TRAP^+$ cells were abundant on day 10 after fracture and the number peaked on day 14. In the CLD-lip group, significantly fewer $TRAP^+$ cells were observed at days 14 and 21 after fracture compared to the PBS-lip group. Fewer $TRAP^+$ cells were also observed in non-fractured areas of the bone in the CLD-lip group as compared to the PBS-lip group (data not shown).

Clodronate Liposome Treatment Impairs Femur Fracture Healing in Mice

μCT analysis was also performed on a subset of the PBS-lip and CLD-lip treated mice at each time point (3 mice per time point per treatment). Sagittal views from the center of each callus were compared (Figure 2A–D). In mice treated with PBS-lips, bridging of the fracture with woven bone was evident by 14 days after fracture (Figure 2A). By 21 days after fracture, callus size appeared to be reduced in the PBS-lips treated mice indicating that callus remodeling had occurred (Figure 2B). Apparent differences were observed in CLD-lip treated mice on day 14 and 21 after fracture. At 14 days after fracture in CLD-lip treated mice, some woven bone was evident at the peripheral edges of the callus (Figure 2C). However, the central portion of the callus lacked X-ray dense material indicating that this portion of the callus was filled with soft tissue. By 21 days, fractures were still not bridged in the CLD-lip treated mice with a clear gap in the callus still evident (Figure 2D).

Plain radiographs of resected femurs were assessed to determine the extent of callus bridging using a previously established 0 to 4 point scoring system (Figure 2E). Healing appeared to progress normally in the PBS-lip treated mice with apparent complete callus bridging occurring by 21 days after fracture. In contrast, apparent callus bridging was significantly reduced at all time points in the CLD-lip treated mice.

Torsional mechanical testing confirmed that CLD-lip treatment impaired healing (Table 1). Femurs were resected 28 days after fracture and tested to failure in torsion as previously described[14]. Consistent with the larger callus dimensions in the CLD-lip treated mice and apparent partial bridging of the fracture callus (Table 1 and Figures 2E and 3E), callus structural properties (peak torque and maximum rigidity) were similar between PBS-lip and CLD-lip treated mouse calluses. In contrast, callus material properties (maximum shear stress and shear modulus) were significantly reduced in the CLD-lip treated mouse calluses.

Clodronate Liposome Treatment Delays Callus Cartilage Resorption

Histological sections of fracture calluses collected at 10 (not shown), 14, and 21 days after fracture were stained with safranin-O to identify cartilage (Figure 3). Large areas of fibrous tissue filled with mesenchymal cells were seen adjacent to the safranin-O stained callus cartilage in the CLD-lip group on days 14 and 21 after fracture but not in the PBS-lip group.

On day 21 post fracture, fractures appeared healed and remodeled in the PBS-lip group with no cartilage apparent within the callus. In comparison, fracture calluses from CLD-lip group appeared to show less bone formation at day 14 (Figure 3C). By 21 days after fracture, the CLD-lip group showed persistence of cartilage within the callus and bone formation in the peripheral edge of the callus (Figure 3D).

Histomorphometry was performed on the histological sections. Callus size and bone area and cartilage area as a percentage of total callus area were measured using images collected from trichrome stained and safranin-O stained sections, respectively (Figure 3E–G). No significant effect of CLD-lip treatment on callus area was detected by ANOVA ($P = 0.102$). However, direct comparison of the day 21 callus areas found that the CLD-lip group (12.3 ± 3.6 mm^2) was significantly greater than the PBS-lip group (6.6 ± 3.3 mm^2; $P = 0.017$, t-test). ANOVA identified significant differences in callus percent bone ($P < 0.001$) and percent cartilage ($P < 0.001$). Callus percent bone area was higher at 21 days after fracture than at 10 or 14 days ($P < 0.001$), but no significant difference between the PBS-lip and CLD-lip groups was found at any time point. In the PBS-lip group, callus cartilage area was greatest at 10 days after fracture before becoming undetectable by 21 days ($P < 0.001$ vs. 10 or 14 day time points). In contrast, callus cartilage area increased from 10 to 14 days in the CLD-lip treatment group ($P = 0.013$) before decreasing at 21 days after fracture ($P \leq 0.003$ vs. 10 or 14 day time points). Cartilage area was different between the PBS-lip and CLD-lip groups at day 14 after fracture ($P = 0.012$).

DISCUSSION

The results of systemic CLD-lip treatment indicate that callus osteoclasts are important for endochondral ossification during fracture healing. The reduction in callus osteoclasts was associated with impaired callus remodeling and with delayed callus cartilage resolution in support of the study hypothesis. The impaired cartilage resolution appeared to limit callus endochondral ossification leading to impaired fracture healing (Figures 2 and 3, Table 1). Callus bone volume is a function of bone formation and resorption. Since bone remodeling is impaired in the CLD-lip treated mice, the similar levels of callus bone observed between the PBS-lip and CLD-lip groups (Figure 3G) support the conclusion that callus endochondral ossification is inhibited in the CLD-lip treated mice. Reduction in callus osteoclasts by RANK:Fc or denosumab treatment also prevents callus cartilage resolution in other fracture models[6; 19]. An obvious potential mechanism is simply that osteoclast activity is necessary to resorb callus cartilage. However, in so doing, the osteoclasts would remove the substratum onto which osteoblasts secrete osteoid. Indeed, an elevated callus osteoclast population has been associated with rapid callus cartilage resorption and impaired fracture healing in streptozotocin-induced diabetic mice[20]. In contrast, inhibition of osteoclast bone resorptive activity by cathepsin K inhibition with odanacatib did not reduce the number of osteoclasts in the callus or prevent resolution of callus cartilage in a rabbit ulna osteotomy[8]. Similar results were observed during femur fracture healing in *Ctsk* null mice[21]. In unfractured bone, targeted deletion of *Ctsk* in mouse osteoclasts increased bone mass even though osteoclast numbers were elevated[22]. These results could be accounted for by at least 3 possibilities. First, an osteoclast resorptive activity that does not require cathepsin K could be responsible for callus cartilage resorption. For example, growth plate cartilage resolution

and bone growth are normal in mice lacking *Dock5* even though bone resorption is impaired[23]. Conversely, callus cartilage resolution is impaired by alendronate treatment, which inhibits the mevalonate pathway in osteoclasts and can inhibit matrix metalloproteinase activity required for callus cartilage resolution[5–8; 24; 25]. Second, an osteoclast-subtype not specifically involved in bone resorption, such as chondroclasts or septoclasts, is responsible for callus cartilage resolution[26]. Third, an unidentified osteoclast activity is required for promoting callus cartilage resolution. For instance, recent studies have indicated that during the reversal phase of bone remodeling, canopy cells associated with osteoclasts are the source of pre-oste oblasts necessary for bone formation[27; 28]. Furthermore, glucocorticoid treatment appears to reduce the association of canopy cells with osteoclasts which may underlie bone loss associated with glucocorticoid use and demonstrates that bone resorption and reversal can be de-coupled[29]. In fracture healing, osteoclasts may not be necessary for specifically resorbing the callus cartilage matrix but may be necessary for recruiting pre-osteoblasts to the site of endochondral ossification as canopy cells. Thus, when osteoclast resorption is inhibited without reducing callus osteoclast numbers, callus cartilage resolution and endochondral ossification still occur because the resorption-impaired osteoclasts can still recruit pre-osteoblasts as canopy cells for bone formation. However, when osteoclasts are absent, cartilage resolution and endochondral ossification are impaired because there are no osteoclasts to recruit pre-osteoblasts for bone formation.

A limitation of the present experimental approach is that the CLD-lips may have had a direct effect on the chondrocyte differentiation or progression into hypertrophy. However, other studies using models of impaired osteoclast activity also noted delayed resolution of callus cartilage. Specifically, fractures in mice homozygous for null mutation of *Dap12* have fewer callus osteoclasts and delayed resolution of callus cartilage[30]. Further, RANK:Fc or denosumab treatment that reduces osteoclast numbers by inhibiting RANKL also causes a delay in callus cartilage resolution[6; 19; 31]. Thus in 3 different approaches that reduced callus osteoclast populations, callus cartilage resolution was impaired. Therefore, it is unlikely the delayed cartilage resolution observed in the CLD-lip treated mice is caused by a direct effect of the CLD-lips on chondrocytes.

Determining the precise role and mechanism by which callus osteoclast promote fracture healing will require additional experimentation. Functional interaction between osteoblasts and osteoclasts is well established for promoting osteoclastogenic activity[32]. Conversely, a recent study showed that sphingosine-1-phosphate production by osteoclasts promotes osteoblast activity and bone formation in mice[22]. Similarly, osteoclasts were found to produce sphingosine-1-phosphate, BMP-6, and Wnt10b in vitro that stimulated osteoblast activity[33]. Other studies also have suggested or demonstrated functional interactions between osteoclasts and chondrocytes, particularly hypertrophic chondrocytes, during endochondral ossification. Hypertrophic chondrocytes produce VEGF which can stimulate osteoclast activity and inhibition of VEGF impairs osteoclast resorption of cartilage during endochondral ossification[34–37]. Chondrocytes also can express RANKL and OPG to control osteoclast formation during endochondral ossification[38; 39]. Finally, a recent study suggests that Ephrin B2 expression by chondrocytes is important for promoting osteoclast activity and resolving cartilage during endochondral ossification[40].

A critical limitation of this experimental approach is that CLD-lip treatment reduces both osteoclast and macrophage populations[41]. Therefore, these experiments do not specifically distinguish between the effects of reduced osteoclasts, macrophages, or both. Several reports support a role for macrophages in promoting bone formation and fracture callus formation[42–45]. Indeed, Raggat et al. reported that femur fracture callus formation is prevented when macrophages are depleted in the macrophage Fas-induced apoptosis (MAFIA) mouse model co-incident with fracture production, though osteoclasts also should have been depleted[46; 47]. In contrast, fracture callus formation was not affected in the CLD-lip treated mice (Figure 2). If both models equally depleted macrophages and osteoclasts, then callus formation should have been inhibited in both models. As this did not occur, the 2 methods for macrophage and osteoclast depletion must have produced different effects on the efficiency of target cell depletion or the duration of depletion. Cho et al. showed that depletion of monocyte-derived cells by CLD-lip treatment or by using the MAFIA mouse model had significantly different effects on skeletal homeostasis[48]. Induction of target cell apoptosis in the MAFIA mice caused a reduction in tibia fractional bone volume that was refractory to the anabolic effects of PTH treatment. However, CLD-lip treatment caused a small but significant increase in tibia fractional bone volume and the CLD-lip treated mice responded to PTH treatment by almost doubling fractional bone volume. Cho et al. also found that several genes were differentially expressed in the bone marrow of the 2 mouse models that would be consistent with the increased bone formation observed in the CLD-lip treated mice. Whether the differences in fracture healing phenotype between the 2 models relates to specific effects on gene expression, differences in target cell depletion efficacy, or differential depletion of monocytes, macrophages, tissue resident macrophages, and osteoclasts will require additional experimentation. Still, all the experimental results support a critical role for monocyte-derived cells in promoting bone regeneration.

Distinguishing between macrophages and osteoclasts can be challenging[49]. Common phenotypic markers used to detect macrophages are also expressed by osteoclasts. For instance, both cell types express TRAP, colony stimulating factor-1 receptor (*Csf1r*), and EMR-1 (F4/80 antigen). Morphological criteria can distinguish the 2 cell types since osteoclasts are multi-nucleated and are usually found associated with sites of bone or cartilage resorption. Practically, artifacts associated with tissue processing and sectioning for histology can make using morphological criteria to assign the identity of $TRAP^+$ cells as macrophages or osteoclasts difficult. Thus defining the roles that macrophages, tissue resident osteal macrophages, and osteoclasts may have in bone growth, homeostasis, and repair will require more precise tools for analyzing each cell population.

Supplementary Material

Refer to Web version on PubMed Central for supplementary material.

ACKNOWLEDGEMENTS

Research reported in this publication was supported by the Department of Defense Congressionally Directed Medical Research Programs Peer Reviewed Orthopaedic Research Program under award number W81XWH-10-1-0944 to JPOC. HNL and JPOC have no conflicts of interests.

REFERENCES

1. Lin HN, O'Connor JP. 2014 Immunohistochemical localization of key arachidonic acid metabolism enzymes during fracture healing in mice. PloS one 9:e88423. [PubMed: 24516658]
2. Rivollier A, Mazzorana M, Tebib J, et al. 2004 Immature dendritic cell transdifferentiation into osteoclasts: a novel pathway sustained by the rheumatoid arthritis microenvironment. Blood 104:4029–4037. [PubMed: 15308576]
3. Sabokbar A, Fujikawa Y, Neale S, et al. 1997 Human arthroplasty derived macrophages differentiate into osteoclastic bone resorbing cells. Annals of the rheumatic diseases 56:414–420. [PubMed: 9486003]
4. Udagawa N, Takahashi N, Akatsu T, et al. 1990 Origin of osteoclasts: mature monocytes and macrophages are capable of differentiating into osteoclasts under a suitable microenvironment prepared by bone marrow-derived stromal cells. Proceedings of the National Academy of Sciences of the United States of America 87:7260–7264. [PubMed: 2169622]
5. Russell RG. 2015 Pharmacological diversity among drugs that inhibit bone resorption. Current opinion in pharmacology 22:115–130. [PubMed: 26048735]
6. Gerstenfeld LC, Sacks DJ, Pelis M, et al. 2009 Comparison of effects of the bisphosphonate alendronate versus the RANKL inhibitor denosumab on murine fracture healing. Journal of bone and mineral research : the official journal of the American Society for Bone and Mineral Research 24:196–208.
7. Soung do Y, Gentile MA, Duong LT, et al. 2013 Effects of pharmacological inhibition of cathepsin K on fracture repair in mice. Bone 55:248–255. [PubMed: 23486186]
8. Pennypacker BL, Gilberto D, Gatto NT, et al. 2016 Odanacatib increases mineralized callus during fracture healing in a rabbit ulnar osteotomy model. Journal of orthopaedic research : official publication of the Orthopaedic Research Society 34:72–80. [PubMed: 26178170]
9. Yu YY, Lieu S, Hu D, et al. 2012 Site specific effects of zoledronic acid during tibial and mandibular fracture repair. PloS one 7:e31771. [PubMed: 22359627]
10. McDonald MM, Dulai S, Godfrey C, et al. 2008 Bolus or weekly zoledronic acid administration does not delay endochondral fracture repair but weekly dosing enhances delays in hard callus remodeling. Bone 43:653–662. [PubMed: 18582604]
11. van Rooijen N, van Nieuwmegen R. 1984 Elimination of phagocytic cells in the spleen after intravenous injection of liposome-encapsulated dichloromethylene diphosphonate. An enzyme-histochemical study. Cell and tissue research 238:355–358. [PubMed: 6239690]
12. Van Rooijen N, Sanders A. 1994 Liposome mediated depletion of macrophages: mechanism of action, preparation of liposomes and applications. Journal of immunological methods 174:83–93. [PubMed: 8083541]
13. van Rooijen N, van Kesteren-Hendrikx E. 2002 Clodronate liposomes: perspectives in research and therapeutics. Journal of liposome research 12:81–94. [PubMed: 12604042]
14. Manigrasso MB, O'Connor JP. 2004 Characterization of a closed femur fracture model in mice. Journal of orthopaedic trauma 18:687–695. [PubMed: 15507822]
15. Al-Zube L, Breitbart EA, O'Connor JP, et al. 2009 Recombinant human platelet-derived growth factor BB (rhPDGF-BB) and beta-tricalcium phosphate/collagen matrix enhance fracture healing in a diabetic rat model. Journal of orthopaedic research : official publication of the Orthopaedic Research Society 27:1074–1081. [PubMed: 19170096]
16. Engesaeter LB, Ekeland A, Langeland N. 1978 Methods for testing the mechanical properties of the rat femur. Acta Orthopaedica Scandanavia 49:512–518.
17. Ekeland A, Engesaeter LB, Langeland N. 1981 Mechanical properties of fractured and intact rat femora evaluated by bending, torsional and tensile tests. Acta orthopaedica Scandinavica 52:605–613. [PubMed: 7331797]
18. Bergenstock M, Min W, Simon AM, et al. 2005 A comparison between the effects of acetaminophen and celecoxib on bone fracture healing in rats. Journal of orthopaedic trauma 19:717–723. [PubMed: 16314720]

19. Flick LM, Weaver JM, Ulrich-Vinther M, et al. 2003 Effects of receptor activator of NFkappaB (RANK) signaling blockade on fracture healing. Journal of orthopaedic research : official publication of the Orthopaedic Research Society 21:676–684. [PubMed: 12798068]
20. Kayal RA, Tsatsas D, Bauer MA, et al. 2007 Diminished bone formation during diabetic fracture healing is related to the premature resorption of cartilage associated with increased osteoclast activity. Journal of bone and mineral research : the official journal of the American Society for Bone and Mineral Research 22:560–568.
21. Gentile MA, Soung do Y, Horrell C, et al. 2014 Increased fracture callus mineralization and strength in cathepsin K knockout mice. Bone 66:72–81. [PubMed: 24928497]
22. Lotinun S, Kiviranta R, Matsubara T, et al. 2013 Osteoclast-specific cathepsin K deletion stimulates S1P-dependent bone formation. The Journal of clinical investigation 123:666–681. [PubMed: 23321671]
23. Touaitahuata H, Cres G, de Rossi S, et al. 2014 The mineral dissolution function of osteoclasts is dispensable for hypertrophic cartilage degradation during long bone development and growth. Developmental biology 393:57–70. [PubMed: 24992711]
24. Colnot C, Thompson Z, Miclau T, et al. 2003 Altered fracture repair in the absence of MMP9. Development 130:4123–4133. [PubMed: 12874132]
25. Behonick DJ, Xing Z, Lieu S, et al. 2007 Role of matrix metalloproteinase 13 in both endochondral and intramembranous ossification during skeletal regeneration. PloS one 2:e1150. [PubMed: 17987127]
26. Odgren PR, Witwicka H, Reyes-Gutierrez P. 2016 The cast of clasts: catabolism and vascular invasion during bone growth, repair, and disease by osteoclasts, chondroclasts, and septoclasts. Connective tissue research 57:161–174. [PubMed: 26818783]
27. Andersen TL, Abdelgawad ME, Kristensen HB, et al. 2013 Understanding coupling between bone resorption and formation: are reversal cells the missing link? The American journal of pathology 183:235–246. [PubMed: 23747107]
28. Delaisse JM. 2014 The reversal phase of the bone-remodeling cycle: cellular prerequisites for coupling resorption and formation. Bonekey Rep 3:561. [PubMed: 25120911]
29. Andreasen CM, Ding M, Overgaard S, et al. 2015 A reversal phase arrest uncoupling the bone formation and resorption contributes to the bone loss in glucocorticoid treated ovariectomised aged sheep. Bone 75:32–39. [PubMed: 25689083]
30. Kamimura M, Mori Y, Sugahara-Tobinai A, et al. 2015 Impaired Fracture Healing Caused by Deficiency of the Immunoreceptor Adaptor Protein DAP12. PloS one 10:e0128210. [PubMed: 26030755]
31. Delos D, Yang X, Ricciardi BF, et al. 2008 The effects of RANKL inhibition on fracture healing and bone strength in a mouse model of osteogenesis imperfecta. Journal of orthopaedic research : official publication of the Orthopaedic Research Society 26:153–164. [PubMed: 17729310]
32. Sims NA, Martin TJ. 2014 Coupling the activities of bone formation and resorption: a multitude of signals within the basic multicellular unit. Bonekey Rep 3:481. [PubMed: 24466412]
33. Pederson L, Ruan M, Westendorf JJ, et al. 2008 Regulation of bone formation by osteoclasts involves Wnt/BMP signaling and the chemokine sphingosine-1-phosphate. Proceedings of the National Academy of Sciences of the United States of America 105:20764–20769. [PubMed: 19075223]
34. Engsig MT, Chen QJ, Vu TH, et al. 2000 Matrix metalloproteinase 9 and vascular endothelial growth factor are essential for osteoclast recruitment into developing long bones. The Journal of cell biology 151:879–889. [PubMed: 11076971]
35. Gerber H-P, Vu TH, Ryan AM, et al. 1999 VEGF couples hypertrophic cartilage remodeling, ossification, and angiogenesis during endochondral bone formation. Nature medicine 5:623–628.
36. Maes C, Carmeliet P, Moermans K, et al. 2002 Impaired angiogenesis and endochondral bone formation in mice lacking the vascular endothelial growth factor isoforms $VEGF_{164}$ and $VEGF_{188}$. Mech Dev 111:61–73. [PubMed: 11804779]
37. Yang Q, McHugh KP, Patntirapong S, et al. 2008 VEGF enhancement of osteoclast survival and bone resorption involves VEGF receptor-2 signaling and beta3-integrin. Matrix biology : journal of the International Society for Matrix Biology 27:589–599. [PubMed: 18640270]

38. Wang B, Jin H, Shu B, et al. 2015 Chondrocytes-Specific Expression of Osteoprotegerin Modulates Osteoclast Formation in Metaphyseal Bone. Scientific reports 5:13667. [PubMed: 26329493]
39. Wang B, Jin H, Zhu M, et al. 2014 Chondrocyte β-catenin signaling regulates postnatal bone remodeling through modulation of osteoclast formation in a murine model. Arthritis Rheumatol 66:107–120. [PubMed: 24431282]
40. Tonna S, Poulton IJ, Taykar F, et al. 2016 Chondrocytic EphrinB2 promotes cartilage destruction by osteoclasts in endochondral ossification. Development.
41. van Rooijen N, van Kesteren-Hendrikx E. 2003 "In vivo" depletion of macrophages by liposome-mediated "suicide". Methods in enzymology 373:3–16. [PubMed: 14714393]
42. Sinder BP, Pettit AR, McCauley LK. 2015 Macrophages: Their Emerging Roles in Bone. Journal of bone and mineral research : the official journal of the American Society for Bone and Mineral Research 30:2140–2149.
43. Alexander KA, Chang MK, Maylin ER, et al. 2011 Osteal macrophages promote in vivo intramembranous bone healing in a mouse tibial injury model. Journal of bone and mineral research : the official journal of the American Society for Bone and Mineral Research 26:1517–1532.
44. Chang MK, Raggatt LJ, Alexander KA, et al. 2008 Osteal tissue macrophages are intercalated throughout human and mouse bone lining tissues and regulate osteoblast function in vitro and in vivo. Journal of immunology 181:1232–1244.
45. Vi L, Baht GS, Whetstone H, et al. 2015 Macrophages promote osteoblastic differentiation in-vivo: implications in fracture repair and bone homeostasis. Journal of bone and mineral research : the official journal of the American Society for Bone and Mineral Research 30:1090–1102.
46. Burnett SH, Kershen EJ, Zhang J, et al. 2004 Conditional macrophage ablation in transgenic mice expressing a Fas-based suicide gene. Journal of leukocyte biology 75:612–623. [PubMed: 14726498]
47. Raggatt LJ, Wullschleger ME, Alexander KA, et al. 2014 Fracture healing via periosteal callus formation requires macrophages for both initiation and progression of early endochondral ossification. The American journal of pathology 184:3192–3204. [PubMed: 25285719]
48. Cho SW, Soki FN, Koh AJ, et al. 2014 Osteal macrophages support physiologic skeletal remodeling and anabolic actions of parathyroid hormone in bone. Proceedings of the National Academy of Sciences of the United States of America 111:1545–1550. [PubMed: 24406853]
49. Athanasou NA, Quinn J. 1990 Immunophenotypic differences between osteoclasts and macrophage polykaryons: immunohistological distinction and implications for osteoclast ontogeny and function. J Clin Pathol 43:997–1003. [PubMed: 2266187]

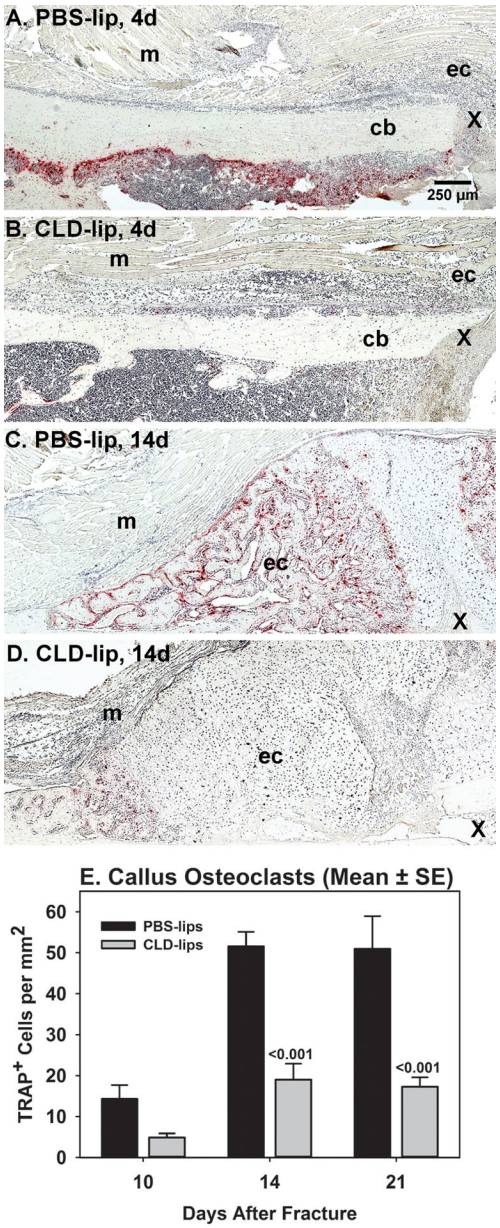

Figure 1. Clodronate liposome treatment reduces fracture callus osteoclasts.

Mouse fracture callus specimens collected at 4, 10, 14, and 21 days after fracture from PBS-lip treated (n= 3, 4, 6, and 6, respectively) and CLD-lip treated (n =3, 5, 6, and 6, respectively) mice were processed for paraffin histology. Shown are sections stained for TRAP activity to identify osteoclasts (red color) at days 4 (A and B) and 14 (C and D) after fracture in PBS-lip (A and C) and CLD-lip (B and D) treated mice. Panels are marked to show the external fracture callus (ec), cortical bone (cb), muscle (m), and fracture site (X). The mean (±SE) number of $TRAP^+$ cells from the 10, 14, and 21 day specimens of the PBS-lip (black) and CLD-lip (gray) treated specimens are shown. Significant differences between treatment groups are noted with associated p values.

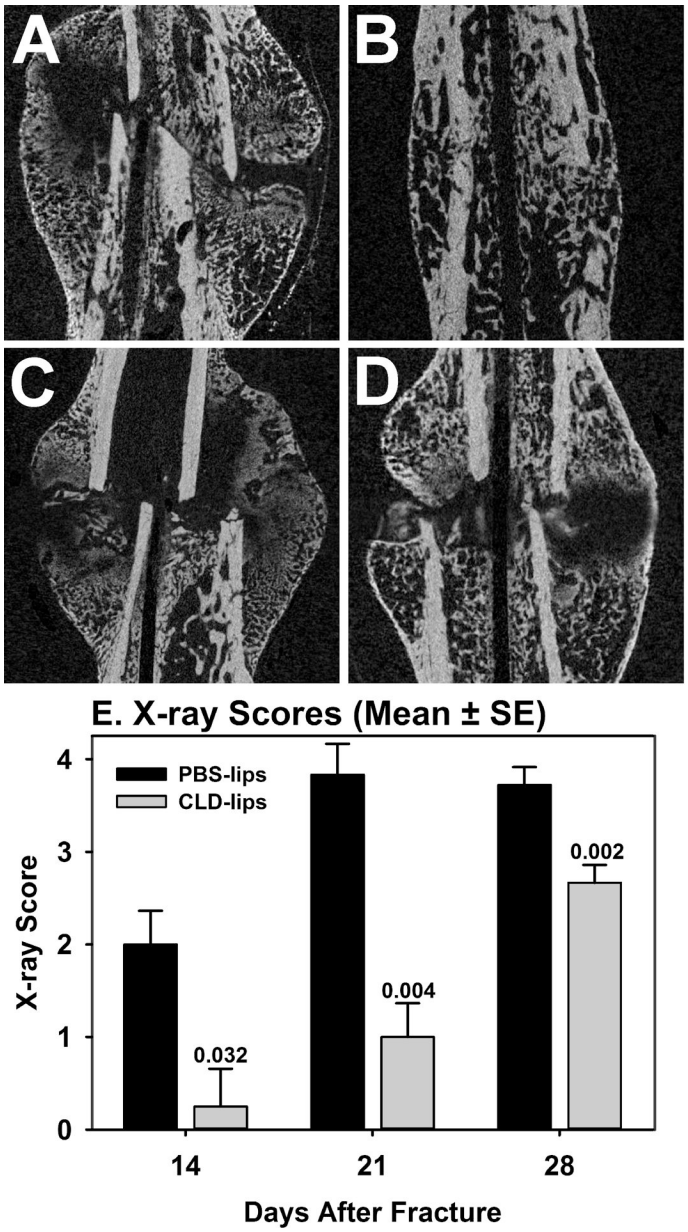

Figure 2. Clodronate liposome treatment impairs fracture healing.

A subset of fracture callus specimens from the PBS-lip and CLD-lip treated mice were analyzed by μCT. Shown are longitudinal sections through the callus and femoral canal for PBS-lip treated (A and B) and CLD-lip treated mice (C and D) at 14 (A and C) and 21 (B and D) days after fracture. Callus specimens collected at days 14, 21, and 28 days after fracture were radiographed and the X-rays were scored to identify and deficit in apparent healing. As shown in E, X-rays scores were significantly lower for the CLD-lip specimens (gray) at all time points as compared to the PBS-lip treated specimens (black).

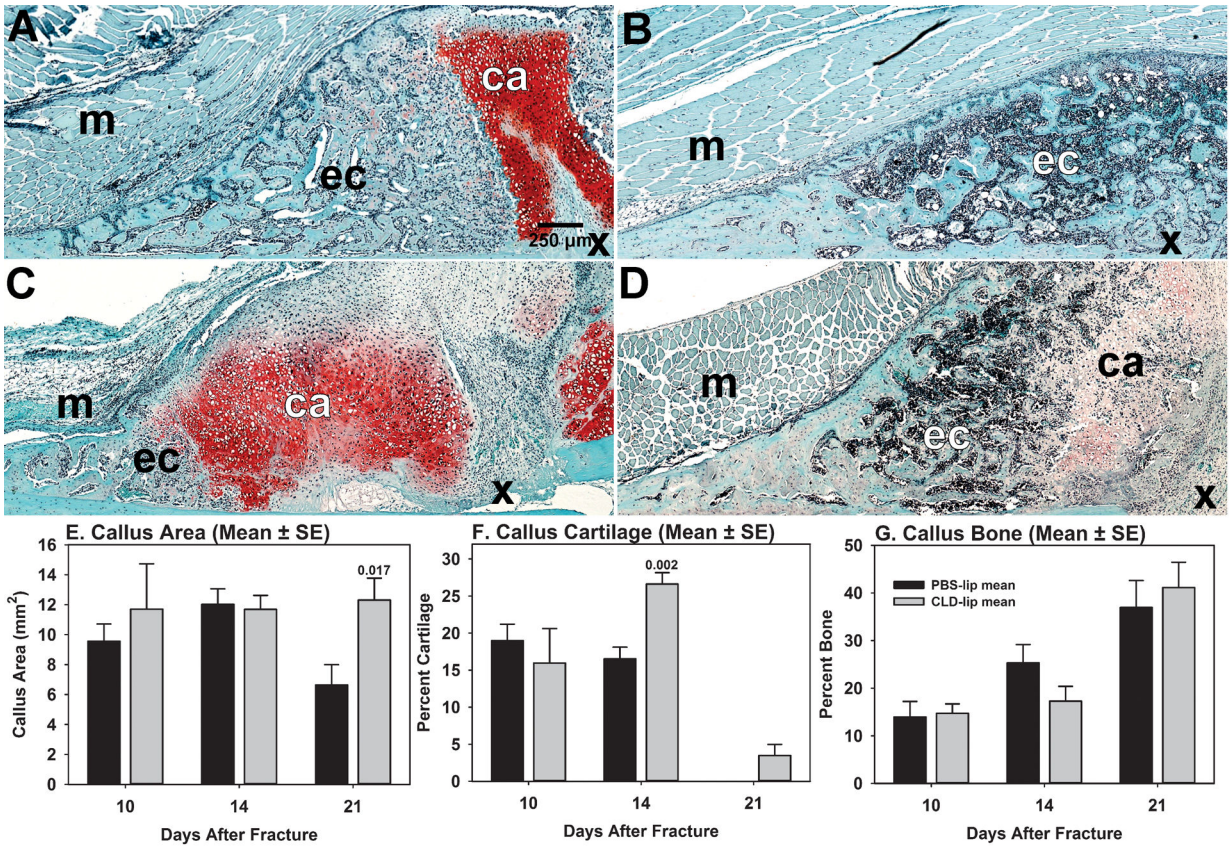

Figure 3. Resolution of callus cartilage is impaired in clodronate liposome treated mice.

Histomorphometry was performed on fracture callus specimens collected at 10, 14, and 21 days after fracture from PBS-lip treated mice (n = 4, 6, and 6, respectively) and from CLD-lip treated mice (n = 5, 6, and 6, respectively). Cartilage was identified by safranin-O staining and histological appearance. Bone was identified by aniline blue staining and histological appearance (not shown). Panels A and B: PBS-lip treated mouse specimens at 14 and 21 days, respectively. Panels C and D: CLD-lip treated mouse specimens at 14 and 21 days, respectively. Shown are callus cartilage (ca), the external fracture callus (ec), muscle (m) and fracture site (X). Callus area (Panel E), callus percent cartilage (Panel F), and callus percent bone (Panel G) were measured from digital images of each specimen and are shown as mean values (± SE) for PBS-lip (black) and CLD-lip (gray) treated mouse specimens. Statistically significant differences between the PBS-lip and CLD-lip treated specimens within a time point are indicated by the associated p value.

Table 1.

Torsional Mechanical Testing Analysis

	N	Max. Callus Diameter (mm)	Polar Moment	Peak Torque (Nmm)	Max. Rigidity (Nmm^2/rad)	Max. Shear Stress (MPa)	Shear Modulus s(MPa)
PBS-Lips	14	3.65±0.15	5.05±0.8	35.3±3.7	3119±358	17.3±3.08	1027±259
CLD-Lips	13	4.56±0.17	15.92±4.6	35.0±4.8	4038±527	6.6±1.08	358±58
P value		<0.001	0.024	0.965	0.156	0.002	0.027